



## Application of a microrheology technique to measure the viscosity of disodium cromoglycate liquid crystal

I. Duchesne, S. Rainville & T. Galstian

**To cite this article:** I. Duchesne, S. Rainville & T. Galstian (2016) Application of a microrheology technique to measure the viscosity of disodium cromoglycate liquid crystal, *Molecular Crystals and Liquid Crystals*, 630:1, 6-18, DOI: [10.1080/15421406.2016.1146861](https://doi.org/10.1080/15421406.2016.1146861)

**To link to this article:** <http://dx.doi.org/10.1080/15421406.2016.1146861>




View supplementary material 



Published online: 01 Jul 2016.



Submit your article to this journal 



Article views: 39



View related articles 



View Crossmark data 

# Application of a microrheology technique to measure the viscosity of disodium cromoglycate liquid crystal

I. Duchesne, S. Rainville, and T. Galstian

Department of Physics, Engineering Physics and Optics, and Center for Optics, Photonics and Lasers, Laval University, Quebec City, Canada

## ABSTRACT

Although the science of rheology is well established, some important challenges still persist to measure the viscoelastic properties of complex fluids, such as biological solutions and liquid crystals (LC). In this work, we present a method, based on the calculation of the step length of Brownian particles, to measure the effective local viscosity sensed by microscopic objects in the LC host. This approach allowed us to quantify the anisotropy of the viscosity, and it could also be extended to measure the local viscosity in other nonhomogeneous media. We also present a new guided light dark-field microscopy technique that was used to track particles during our experiments.


## KEYWORDS

Brownian motion; dark-field microscopy; DSCG; liquid crystal; viscosity

## Introduction

Many biological fluids are complex assemblies of self-aligned polymers and other large molecules. Biofilms and synovial fluid are two good examples. Most of them are said to be non-Newtonian, which means that the shear viscosity depends upon the shear rate. These fluids are generally nonhomogeneous and some of them can exhibit quasi macroscopic anisotropic properties [1–6]. The biological functions of these fluids as well as the behavior of microorganisms that live in these environments are very sensitive to the local physical properties of the host [1–3, 7–11]. It is thus of great importance to characterize non-Newtonian fluids and to understand how their local properties (like the local viscosity) affect the passive diffusion of molecules and the active movements of microorganisms (such as flagellated bacteria) [7–14]. The effective viscosity sensed by microscopic objects in such self-aligned fluids not only has directional dependence (as in liquid crystals (LCs)), but it depends also upon their speed [3,15] and finally, in nonuniform solutions, upon their position [3,16]. Since conventional rheometer techniques measure viscosity by moving a large amount of liquid, they cannot determine the local viscosity. In addition, when the liquid is formed with rod-shaped aggregates that can form a well aligned matrix (such as lyotropic LC), these methods will reorganize or destroy the aggregates and their alignment, thus dramatically changing the viscosity of the medium [17]. Finally, since the conditions in which the conventional viscosity is

**CONTACT** T. Galstian ✉ [tigran.galstian@phy.ulaval.ca](mailto:tigran.galstian@phy.ulaval.ca) Department of Physics, Engineering Physics and Optics, Center for Optics, Photonics and Laser, Laval University, 2375 Rue de la Terrasse, Quebec City (QC), Canada G1V 0A6.  
Color versions of one or more of the figures in the article can be found online at [www.tandfonline.com/gmcl](http://www.tandfonline.com/gmcl).

 Supplemental data for this article can be accessed on the [publisher's website](#).

© 2016 Taylor & Francis Group, LLC

measured are very different from passive or active diffusion of microscopic objects in complex solutions, it would be difficult to use this measurement to model their displacement.

The conventional rheology technique can clearly help to describe the viscoelastic properties of complex media, but microrheology techniques are needed to complete this characterisation [18–21]. In this report, a low-cost method based on the Brownian motion of microspheres is revisited for measuring viscosity. These measurements are based on the calculation of the step length (SL) rather than the conventional mean square displacement (MSD) of Brownian particles since a previous report has shown that this method is more accurate when a small number of step is used [22]. This technique can be used to model the effective viscosity sensed by microscopic objects that move slowly in non-Newtonian fluids. It also allows the measurements of local viscosity and its anisotropy. In the present work, this analysis is first tested by using Newtonian solutions of sucrose with known viscosity (as a reference) and is then applied to water solutions of disodium cromoglycate (DSCG), which is a lyotropic LC. A new microscopy technique is also presented and qualitatively characterized. This technique, named “guided light dark-field” (GLDF) microscopy, was specifically used to perform the viscosity measurements in DSCG solutions.

## Theory

### Viscosity calculation

To measure the viscosity of our solutions, a technique similar to that described in [22] was used (with known size of microspheres rather than known viscosity). Below, a similar derivation to that found in [22] is described, but for one dimension only. From the theory of Brownian motion in one dimension, the number of particles ( $dn$ ) that execute a given squared step length (SSL) in a fixed time interval ( $\Delta t$ ) is described by the following density probability

$$P(SSL, \Delta t) = \frac{dn}{dSSL} = \frac{1}{2D\Delta t} e^{-\frac{SSL}{2D\Delta t}}, \quad (1)$$

where  $D$  is the diffusion coefficient. For a spherical particle in a fluid,  $D$  can be determined by the following expression [18]

$$D = \frac{kT}{3\pi\eta d}, \quad (2)$$

where  $k$  is the Boltzmann constant,  $T$  is the temperature in Kelvin and  $d$  is the diameter of the particle. The Eq. (1) has the form of an exponential distribution. The average squared step length  $\langle SSL \rangle$  is given by

$$\langle SSL \rangle = 2D\Delta t. \quad (3)$$

The probability to obtain  $n$  particles within the interval  $dn$  of step length  $SL$  within the interval  $dSL$  and time interval  $\Delta t$  can be mathematically derived from Eq. (1):

$$P(SL, \Delta t) = \frac{dn}{dSL} = \frac{dn}{dSSL} \frac{dSSL}{dSL} = 2SL \frac{dn}{dSSL}, \quad (4)$$

so that

$$P(SL, \Delta t) = \frac{SL}{D\Delta t} e^{-\frac{SL^2}{2D\Delta t}}. \quad (5)$$

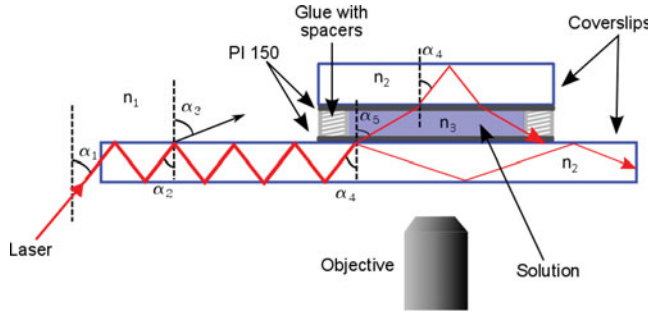


**Figure 1.** Scheme of a chamber used for the observation of probe microspheres. The principle of GLDF microscopy is also illustrated (see details in the text).

This equation has the same form as the Rayleigh distribution equation with the mean of the distribution of  $SL$  given by the following expression

$$SL = \sqrt{\frac{\pi D \Delta t}{2}} . \quad (6)$$

By using the Eq. (2) we obtain

$$SL = \sqrt{\frac{kT \Delta t}{6\eta d}} , \quad (7)$$

from which we finally obtain the equation for the viscosity in terms of the mean step  $SL$  length in a given time interval  $\Delta t$ :

$$\eta = \frac{kT \Delta t}{6d SL^2} . \quad (8)$$

### Guided light dark-field microscopy principle

GLDF microscopy was used to visualize the Brownian motion of microspheres. In this technique, a laser beam is injected into the edge of a coverslip and initially remains trapped inside (Fig. 1). When light enters the sandwich-like chamber containing the solution, it can escape the coverslip, but it remains trapped in the chamber (between the two coverslips). The light scattered by the objects (microparticles) in the solution is then the only light that can escape and be collected by the objective (perpendicular to coverslips), as in conventional dark-field microscopy.

For this technique to work properly, the light beam must be injected into the coverslip at a well-defined angle that is calculated here. First, we have to calculate the critical angle for each interface. These angles can be obtained by using the well-known Snell-Descartes law

$$\alpha_c = \sin^{-1} \frac{n_t}{n_i} , \quad (9)$$

where  $n_i$  is the refractive index of the medium where the light come from and  $n_t$ , the refractive index of the second medium. If we suppose  $\alpha_1$  is between 0 and  $90^\circ$  with  $n_1 = 1$ ,  $n_2 = 1.51$  and  $n_3 = 1.33$  we obtain the following critical angles (Fig. 1):

- $\alpha_{2c} = 41.47^\circ$  (light rays injected at angles between  $41.47^\circ$  and  $90^\circ$  will remain in the guide in the area of glass–air interfaces),
- $\alpha_{4c} = 61.74^\circ$  (light rays injected at angles between  $41.47^\circ$  and  $61.74^\circ$  will enter the water–solution when reaching the glass–water interface).

Then we can calculate what will be the angle of penetration in water:

- $\alpha_5 = 48.75^\circ$  ( $\alpha_4 = 41.47^\circ$ ) to  $90^\circ$  ( $\alpha_4 = 61.74^\circ$ ).

In the case where the injector is coupled to the coverslips (glass–glass interface) the injection angle ( $\alpha_1$ ) should be between  $41.47^\circ$  and  $61.74^\circ$ . For an air coupled injector (air–glass interface) the injection angle should be between  $0^\circ$  and  $44.37^\circ$ , which correspond to guided angles ( $\alpha_4$ ) between  $48.53^\circ$  and  $61.74^\circ$ . It is important to note that this technique can be used with any dry objectives, but the presence of water or oil between the coverslip and the objective would allow the light to enter directly into the objective, thereby creating an enormous background signal.

## Materials and methods

### Bacterial culture

*E. coli* strain HCB33 (wild type) (obtained from the laboratory of Howard Berg) was used exclusively to test the GLDF technique on passive (bacteria stuck on one surface) and active (swimming bacteria) anisotropic objects (oblong shape). Bacteria were first grown on agar plate (15 g agar, 10 g Bacto-Tryptone and 5 g NaCl in 1 liters) at  $37^\circ\text{C}$  for 24 hr. Bacteria from a single colony were then selected from this plate and grown overnight to saturated phase at  $34^\circ\text{C}$  in a shaking incubator at 200 rpm. The saturated culture was then diluted by a factor of 10 in motility buffer (MB) (10 mM  $\text{KPO}_4$ , 0.1 mM EDTA and 10 mM lactic acid) and a small amount of this mixture was injected directly in the chamber for observation.

### Sucrose solution

To estimate the precision of our viscosity measurements, solutions of sucrose with known viscosity were used as reference [19]. Various quantities of sucrose were added to deionized (DI) water containing microspheres with diameters ranging from  $0.2\text{ }\mu\text{m}$  to  $2\text{ }\mu\text{m}$  (see Table S1 for more information) to obtain solutions with a volume around 2 ml and concentrations of sucrose of 0 wt%, 47 wt%, or 63 wt%. Since the reference viscosity has been measured at  $20^\circ\text{C}$ , the heating and cooling stage HCMIS and TC-10 controller (from ALA scientific instrument, Farmingdale, NY) were used to control the temperature of the sample. To do so, two temperature probes were used: one (the reference probe) was directly fixed onto the upper surface of the chamber and the other one was inserted inside the stage. The temperature on the top of the chamber was observed to change by at most  $\pm 0.3^\circ\text{C}$  ( $20 \pm 0.3^\circ\text{C}$ ), but the temperature indicated by the probe inside the stage varied between  $18^\circ\text{C}$  and  $21^\circ\text{C}$ .

### DSCG LC solution

The well-known asthma drug DSCG (Sigma-Aldrich C0399, St. Louis, MO) was used to make the LC solutions [20]. To obtain various concentrations of DSCG LC, a concentrated solution was first made by adding 16 wt% of DSCG to 84 wt% of DI water. To solubilize the DSCG completely, this mixture was heated for at least 10 min at  $55^\circ\text{C}$  and then agitated for about 1 min. The concentrated solution was stored at  $4^\circ\text{C}$  and discarded after one week. This solution was always heated at  $55^\circ\text{C}$  for 5 min and then shaken for 1 min for homogeneity just before each use. A small amount of the concentrated LC was then diluted into a suspension with a total volume of  $160\text{ }\mu\text{L}$  containing polystyrene microspheres with diameters between  $0.2\text{ }\mu\text{m}$  and  $2\text{ }\mu\text{m}$  (see Table S1) to obtain a DSCG concentration from 0 wt% to 13.7 wt%. All

our experiments in DSCG LC were made at room temperature ( $22.5 \pm 0.5^\circ\text{C}$ ). In this condition, DSCG creates a nematic LC phase above 11 wt% and isotropic phase below 10 wt%. Between 10 wt% and 11 wt% both phases coexist.

### **Observation chamber**

To study our solutions, a custom optical chamber was used. To fabricate this chamber, two coverslips were covered by spin coating with a layer of PI-150 at 1% (Nissan Chemical B79032-50, Houston, TX). These surfaces were then rubbed in opposite directions by using the technique explained in [23]. A cavity was finally formed by joining together two coverslips with periphery UV glue (Norland, Optical Adhesive 65, Cranbury, NJ) containing 30  $\mu\text{m}$  or 60  $\mu\text{m}$  glass beads used as spacers (Duke Scientific Corporation 9030 and 9060, Palo Alto, CA) (Fig. 1). The final solution was injected into the chamber by capillarity. The chamber was sealed with transparent nail polish to prevent fluid movements and water evaporation. Viscosity measurements for each increment of concentration were acquired from at least 3 different samples made from at least 2 different stock solutions.

### **Visualization technique**

GLDF microscopy was used to visualize particles in all samples except the sucrose solutions that were observed in bright field microscopy (since GLDF microscopy is incompatible with our heating and cooling stage). The injector from the lightguide-based Total Internal Reflection Fluorescence Microscope from TIRF Technologies (Morrisville, NC) was used to inject the light into the coverslip. A laser with a wavelength of 473 nm and a power of 550 mW (TIRF Technologies) was used to illuminate the sample. To test the impact of noncoherent light (white light) on the acquired images, the X-Cite 120 XL lamp from EXFO (Quebec, Canada) was also used for illumination. To detect the microspheres, a 50x objective with 0.5 NA (Olympus LMPLFLN 50X, Tokyo, Japan) was employed. The EMCCD iXon3 888 camera (Andor Technology, South Windsor, CT) mounted on an IX71 microscope (Olympus) was used to record images of the samples. Images of microspheres with diameter varying from 0.2  $\mu\text{m}$  to 3  $\mu\text{m}$  or bacteria (in water) were recorded to characterize the light pattern scattered by objects with different shapes and sizes.

### **Viscosity measurements**

The Brownian motion of polystyrene beads was used to measure the viscosity of solutions of DSCG or sucrose. The concentration of microspheres was chosen to rapidly acquire good statistics, while limiting the particle's aggregation (see Tables S1 and S2). Our analysis algorithm excluded the trajectories where two microspheres came too close to each other (about 2  $\mu\text{m}$ ). In the anisotropic phase of DSCG LC, the concentration was an order of magnitude lower to prevent inter-particle interactions (due to elastic forces). A previous report has shown that particles interact with each other when the distance between them is smaller than 3 particle diameters for tangential surface alignment (as for our particles) and with a LC with similar elasticity constants than those of the DSCG [24,25]. As we can see in Table S2, the mean distance between particles is always much higher than this limit. Videos containing 100 frames were recorded by a custom LabVIEW program (National Instruments,

Austin, TX) at an acquisition rate varying from 6.7 fps to 1/6 fps (depending upon the diameter of microspheres and the concentration of DSCG or sucrose) and an exposure time of 33 ms.

Videos of the microspheres diffusion were analyzed with a custom particle-tracking algorithm in the MATLAB computing environment (MathWorks, Natick, MA). The position of every particle in each frame was determined by identifying the center of a Gaussian function fitted on the signal recorded by the CCD. The precision on the position was better than 100 nm. To obtain the viscosity of the host medium, the SL was first computed for each particle as the absolute value of the difference between its position in two consecutive images ( $|\Delta p| = \sqrt{\Delta x^2 + \Delta y^2}$ ). Then, the possible directional drift of the sample was corrected separately in every movie by removing from each position the mean of  $\Delta p$  calculated for every microspheres in the movie. Finally, the effective viscosity along the axes parallel ( $x$  axis) and perpendicular ( $y$  axis) to the director ( $\mathbf{n}$ ) (corresponding to the alignment of the aggregates) of DSCG was computed from the average SL of each trajectory using the expressions derived above (Eq. 8). To determine the orientation of the director, the sample was observed between two crossed polarizers. The orientation of the director was then identified as the angle between the  $x$  axis (the rubbing direction) and the polarizers that maximized the transmitted light [26]. To demonstrate that the diffusion of the microsphere was normal at the time scale used for our measurements, the mean squared displacement (MSD) was plotted as a function of time [21,27]. Trajectories with less than 10 frames were discarded. Microspheres with diameters varying from 0.2  $\mu\text{m}$  to 2  $\mu\text{m}$  were used (see Table S1).

## Results and discussion

### *Calibration of the viscosity with sucrose solution*

As mentioned earlier, it is possible to measure the viscosity of a solution by observing the Brownian motion of particles with known size. To estimate the precision of this approach, we measured the viscosity of solutions of sucrose (with determined viscosity) using microspheres with diameters ranging from 0.2  $\mu\text{m}$  to 2  $\mu\text{m}$  (see Table S1). In Fig. 2(B), we can see that the precision of our viscosity measurements is around 12% and the difference between the viscosities recorded from measurements obtained from different size of beads is at most 8% (Fig. 2(C)). However, the precision on the ratio of the viscosities in two perpendicular directions is better, with a value around 4% (Fig. 2(D)).

A priori, we expected this technique to be more precise, but we think that the difference between the measured and the reference viscosities could come from temperature variations. Since it was impossible to insert the reference probe (small thermistor) inside the chamber, this probe was positioned above the surface of the chamber. It is therefore possible that the actual temperature inside the chamber deviated from the value measured with the probe. A second probe that measured the temperature of the heating and cooling element (inside the stage) detected a temperature between 18°C and 21°C, so the temperature inside the chamber could fluctuate at least between these two values. Using these fluctuations, we obtain a possible variation of the viscosity of +4% and -3% in water, +6% and -5% at 47 wt% of sucrose, and +11% and -7% at 63 wt% of sucrose. Temperature fluctuations could therefore explain the majority of the difference between our measurements and the reference values. Since the volume of each solution was relatively large, the uncertainty on the concentration was small (around 0.1 wt%) and should not greatly affect the viscosity. Finally, the measured viscosity of water at room temperature, namely  $(22.5 \pm 0.5)^\circ\text{C}$ , was  $(0.96 \pm 0.01)$  mPa s while the expected



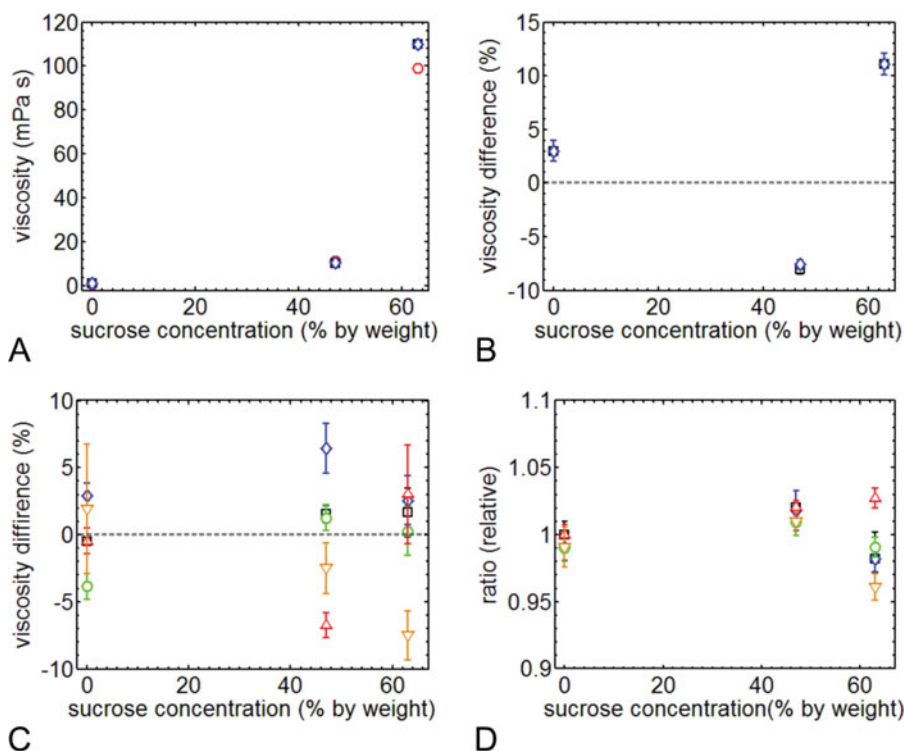


**Figure 2.** Comparison of the reference viscosity (obtained from [28]) with the one measured with 5 sizes of microspheres in solutions of sucrose. (A) Average viscosity, obtained from the measurements performed with microspheres with diameters from  $0.2\ \mu\text{m}$  to  $2\ \mu\text{m}$ , in the x-axis (squares), in the y axis (diamonds) and viscosity obtained from [28] (circle). (B) Relative difference between the reference values and our viscosity measurements in A. (C) Relative difference between the values obtained in A and those measured with each size of microspheres. (D) Ratio of the viscosity along the x axis and the viscosity along the y-axis as a function of the sucrose concentration. Each symbol in (C) and (D) correspond to the viscosity measured with a specific microsphere diameter;  $\square = 0.2\ \mu\text{m}$ ,  $\diamond = 0.5\ \mu\text{m}$ ,  $\circ = 0.75\ \mu\text{m}$ ,  $\triangle = 1\ \mu\text{m}$ , and  $\nabla = 2\ \mu\text{m}$ . The standard errors of the mean (SEM) have been used as uncertainties values.

value is  $(0.95 \pm 0.01)$  mPa s. We conclude that this technique can reach a precision of 1% on viscosity measurements in a well-controlled environment.

### Viscosity of DSCG solution in distilled water

To use our method in a non-Newtonian anisotropic liquid, we measured the viscosity of DSCG solutions with different concentrations. Using the viscosity measurement technique described above (for the sucrose solutions), we found the effective viscosity of solutions of DSCG LC in the direction parallel and perpendicular to the director  $\mathbf{n}$ . We first verified whether the measured viscosity of DSCG solutions depended on the size of the probe microparticles. The section below shows that our measurements are independent of the microspheres' diameter. We therefore averaged the data from all particle sizes to obtain the points reported in Fig. 3.

Using this technique we also measured the viscosity of DSCG solution in Motility buffer (MB) and the results are reported in [11]. By comparing Figs. 3(A) and (B) with data in MB taken from [11], we observe three concentration zones with the same characteristics in both media: (1) a slight increase of the viscosity in the isotropic phase, (2) a fast exponential growth



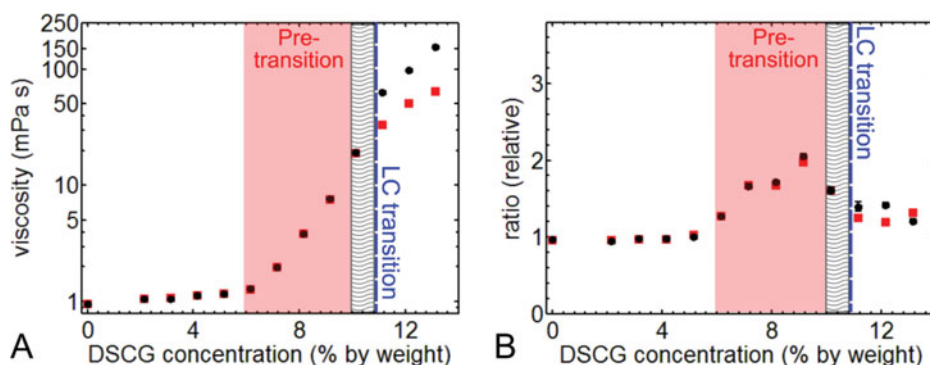


**Figure 3.** Characterization of the effective uniaxial viscosity of DSCG solutions in DI water. (A) Viscosity parallel (squares) and perpendicular to  $\mathbf{n}$  (dots). (B) Ratio of the viscosity of DSCG solution in MB (from [11]) on that of solution in DI water computed from the viscosity parallel (squares) and perpendicular to  $\mathbf{n}$  (dots). The wavy zones represent the region where both the isotropic and nematic phase coexist in the solution. Each point was measured from a data set containing at least 900 microspheres and 40,000 positions; in total, 36,000 individual microspheres were tracked (over 1.20 million positions). The standard error of the mean is used as uncertainties values, but these are generally too small to be visible in figures.

of the viscosity in what we call the pretransition zone (concentration range between 6 wt% and 10 wt%), and (3) a slower exponential growth and appearance of anisotropy of the viscosity in the nematic phase. The anisotropy of the viscosity is similar in both media with a value between 2 and 2.5 in DI water and around 2.2 in MB. As reported in [11], the second zone (exponential increase of the viscosity) happens well before the isotropic-nematic phase transition and is probably caused by the fast increase in the length of the DSCG aggregates. However, the viscosity in MB solutions is at least 20% higher than the one in DI water in that zone and above (see Fig. 3(B)). Interestingly, this difference is more important in the pre-transition zone than in the nematic phase, with a viscosity in MB solutions reaching twice that in DI water at 9.2 wt%. A difference between these two media was expected since the ions in the solvent change the properties of the DSCG solution [29–30], but we are not aware of any study that reported the maximum difference to be in that region (just before the phase transition). Since the DSCG concentration in the two solutions is exactly the same, we think that interactions between the DSCG molecules (i.e., aggregation) are noticeably affected by the presence of ions, causing the change of viscosity. Since the pretransition zone is where the viscosity depends most strongly upon the concentration, it is understandable that it is also in this region that the effect of solvent is most pronounced.

Finally, by comparing the solutions in DI water with those in MB, we observe that the concentration of the LC transition seems to be rather weakly affected by the solvent: solutions at 9.2 wt% were always completely isotropic and those at 10.2 wt% were always a mix of the two phases. However, the ratio of these phases was different: the solutions in DI water show only about 10% of anisotropic fraction compared to approximately 50% in MB solutions. We conclude that the shift in concentration of the LC transition is less than 1 wt% (our concentration increment) and must be around 0.5 wt% based on the comparison of samples from both solutions.

When the bulk velocity of the medium is high enough in the nematic phase, it can in principle perturb the alignment of the DSCG molecule. Since a small drift was observed in our samples, the Ericksen number has been computed [18] to verify whether this drift could perturb the alignment of the DSCG aggregates. The Ericksen number is given by the following

**Table 1.** Ericksen number computed for the drift in the samples in the nematic phase

Concentration ( $\pm 0.2$ ) (wt%)	Mean value for all samples	Maximum value in samples
11.2	0.0009	0.0048
12.2	0.0007	0.0056
13.2	0.0011	0.0022

expression

$$E_r = \frac{\eta v L}{K} \quad (10)$$

where  $\eta$  is the viscosity,  $v$  is the bulk velocity,  $L$  the length scale and  $K$  the elasticity (around 10 pN for DSCG solution [25]). By using a length scale of 1  $\mu\text{m}$ , the drift in the sample as bulk velocity and our viscosity measurements, we found that  $E_r$  was always much smaller than 1 (see Table 1), which means that the drift doesn't perturb the alignment of the aggregates [25].

### Linear correlation between the mean squared displacement (MSD) and time

To make sure that the diffusion of microspheres was always normal, we plotted the MSD as a function of time. A linear relationship was always observed for the first 50 data points (short times) for any size of particles and DSCG concentration (see Fig. 4 for an anisotropic solution and Figure S3 for some others samples). For longer times, the relation was noisier due to a limited number of data and to the spread of the MSD distribution with the time. Indeed, fewer particles were tracked for more than 50 frames because they moved outside of the field of view (as much in the  $z$  direction as in the  $xy$  plane). To quantify the linearity of this relation for various time intervals, the linear coefficient (also known as Pearson product moment coefficient of correlation) between the MSD and time was computed for only the first 10 points and then for 50 points (for each size of particle and DSCG concentration). As we can see in Figs. 5(A) and (B) the relation at short times is strictly linear (a linear coefficient of 1 is a perfect linear relation), which corresponds to normal diffusion. For longer period of time (Figs. 5(C) and (D)), the relation is still linear but noisier. Note also that we do not observe

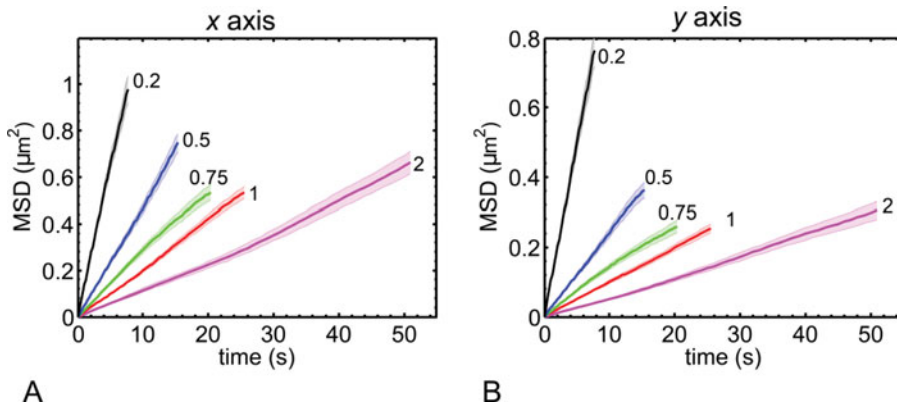


**Figure 4.** MSD versus time for anisotropic solutions with 11 wt% of DSCG. Panel (A) was analyzed from the diffusion in the direction parallel to  $\mathbf{n}$  and panel (B), from the diffusion in the direction perpendicular to  $\mathbf{n}$ . Each color corresponds to the viscosity measured with a specific microsphere diameter; black = 0.2  $\mu\text{m}$ , blue = 0.5  $\mu\text{m}$ , green = 0.75  $\mu\text{m}$ , red = 1  $\mu\text{m}$ , and magenta = 2  $\mu\text{m}$ . The standard errors of the mean (SEM) have been used as uncertainties values.

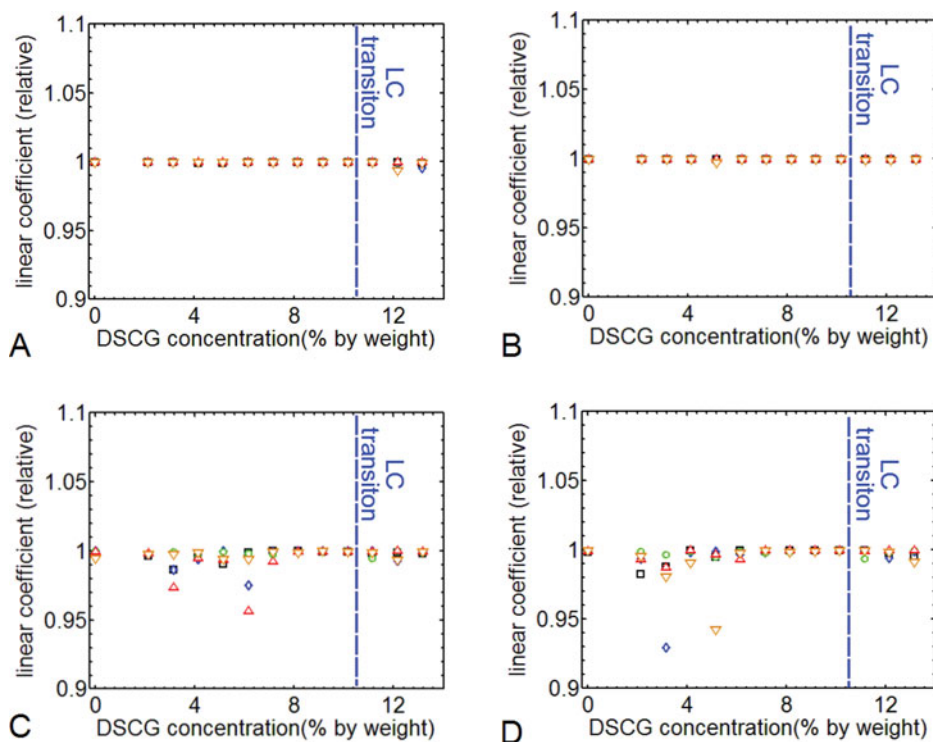


**Figure 5.** Linear coefficient of the MSD versus time showing that the diffusion is normal (at various DSCG concentrations in DI water). In (A) and (B), the linear coefficient was computed from the first 10 data points, while the first 50 points were used in (C) and (D). Panels (A) and (C) correspond to data in the direction parallel to  $\mathbf{n}$  whereas panels (B) and (D) are for data in the direction perpendicular to  $\mathbf{n}$ . For each concentration, the probability to obtain the same coefficient value with a random distribution was estimated to be  $\leq 10^{-15}$ . Each symbol corresponds to the viscosity measured with a specific microsphere diameter;  $\square = 0.2 \mu\text{m}$ ,  $\diamond = 0.5 \mu\text{m}$ ,  $\circ = 0.75 \mu\text{m}$ ,  $\Delta = 1 \mu\text{m}$ , and  $\nabla = 2 \mu\text{m}$ .

any difference in this linear coefficient before and after the LC transition. In reference [21], anomalous diffusion was observed after the LC transition, but our minimum sampling time (0.4 s) was very likely too large for us to observe this effect.

### **Dependence of the measured DSCG viscosity on the size of the microspheres**

To verify whether the measured DSCG viscosity depends on the size of particles used as probes, the DSCG viscosity was measured from the diffusion of polystyrene microspheres of five different diameters at each DSCG concentration. In Fig. 6, the viscosity from each size was normalized by the average viscosity at each DSCG concentration. It is difficult to extract any systematic variation of viscosity with particle size from our measurements, so we averaged the data of all particle sizes together to obtain the points reported in Fig. 3. Since the scatter between the points is on the order of 20%, we can claim that the measured DSCG viscosity varies by at most 20% for particles with a diameter between  $0.2 \mu\text{m}$  to  $2 \mu\text{m}$  and tangential anchoring of the director (measured by polarizing microscope, not shown here).

### **Guided-light dark field microscopy**

To test the GLDF technique we first visualized microspheres with different sizes. As we can see in Fig. 7, the light pattern scattered by the microspheres change with their size. The

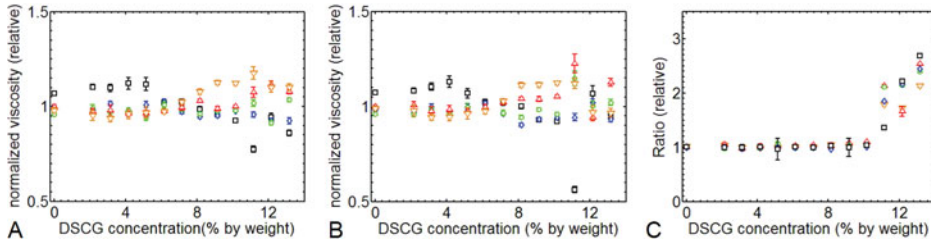


**Figure 6.** Dependence of the measured DSCG viscosity on the size of microspheres. (A) Normalized DSCG viscosity (see text) in the direction parallel and (B) perpendicular to  $\mathbf{n}$  as a function of the DSCG concentration. (C) Ratio of the DSCG viscosity in the direction perpendicular on the viscosity parallel to  $\mathbf{n}$  as a function of the DSCG concentration. Each symbol correspond to the viscosity measured with a specific microsphere diameter;  $\square = 0.2 \mu\text{m}$ ,  $\diamond = 0.5 \mu\text{m}$ ,  $\circ = 0.75 \mu\text{m}$ ,  $\triangle = 1 \mu\text{m}$ , and  $\nabla = 2 \mu\text{m}$ . The SEM is used as uncertainties values.

pattern is symmetric when the particle is smaller than the diffraction limit ( $\sim 500 \text{ nm}$ ) (at  $0.2 \mu\text{m}$ ) but it becomes asymmetric when their diameters are higher (from  $0.5 \mu\text{m}$  to  $3 \mu\text{m}$ ). In this case, the pattern of each microsphere does not change with time since the particles have a spherical shape. However, when some beads aggregate, the light scattered by the aggregates starts to twinkle since the long axis of the cluster rotate with time. Therefore this technique allows the detection of aggregation and it even enables the differentiation of the microspheres sizes by using the directional and temporal dependence of the signal.

We also observed the light scattered by anisotropic objects (rod-shaped bacteria). As we can see in Figs. 8(A)–(C), the pattern is greatly dependent on the orientation of the bacteria. Here again, the intensity of the light twinkles when the bacteria move since its orientation changes. This specificity could be used to record the rotational speed of anisotropic objects. Finally we recorded some images by illuminating the sample with white light (noncoherent) to verify if these patterns were caused by interferences (speckle) or by the orientation of the light rays. As we can see in Fig. 8(D) the pattern does not change by using noncoherent light, so this effect is caused by the orientation of light rays and should be controllable by the injection angle (i.e., the angle at which the light enters the side of the coverslip, namely  $\alpha_1$  in Fig. 1). But the injection angle in our injector is very hard to precisely control, so the possibility of controlling the light pattern by changing the injection angle has not been tested further. It is

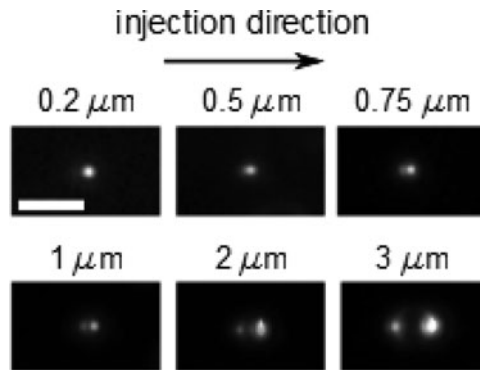


**Figure 7.** Light scattered by microspheres with diameters ranging from  $0.2 \mu\text{m}$  to  $3 \mu\text{m}$  (Table S1) when using GLDF microscopy. The white scale bar measures  $5 \mu\text{m}$ .

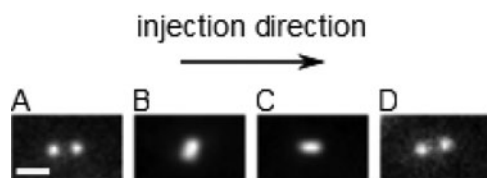


**Figure 8.** Patterns of the light scattered by bacteria with different orientation when using GLDF microscopy. (A) Bacteria in the  $xy$  plane and oriented parallel with the injection, (B) bacteria in the  $xy$  plane and oriented perpendicular with the injection and (C) bacteria tilted in the  $yz$  plane and oriented in the direction of the injection (in the  $xy$  plane). (D) Same as (A) but illuminated with white light. The white scale bar measures  $3\ \mu\text{m}$ .

important to note that this effect cannot be removed since the minimum angle made by the light ray in the sample ( $\alpha_5$  in Fig. 1(B)) is around  $49^\circ$ .

## Conclusion

We have revisited analyses of the Brownian motion of particles by using a new approach to measure the viscosity of complex fluids. This technique can be used to measure local viscosity and its anisotropy. The precision on the measurements is approximately 10% on the absolute value of the viscosity, and 4% on the ratio of viscosities between different axes. By calculating the viscosity with the SL of Brownian motion in DSCG solutions we were able to observe an exponential increase in viscosity with DSCG concentration (that begins in the pretransition zone), and to measure the anisotropy of the viscosity in the LC phase. We also compared the viscosity of DSCG solutions in deionized water and in a MB containing various ions. In both solutions, we observed the same three regimes (purely isotropic, pretransition and anisotropic), but starting in the pretransition zone, the viscosity was at least 20% higher in a MB solution. The largest difference was found to be in the pretransition zone (at 9.2 wt%). This characteristic is not surprising since the physical properties of the media in this zone are very sensitive to the experimental conditions (concentration, temperature, etc.).

We also described a new visualization technique named guided-light dark-field that can be used with any dry objective and laser source. This technique consists in guiding light into a closed chamber with an axial symmetry, so the light collected by the objective is only the one scattered by the micro-objects in solution. We noticed that the light scattering pattern changes with the size, the shape and the orientation of microscopic particles. We postulate that this effect is caused by the tilt of the illumination. This particularity could be advantageously used to differentiate different sizes of spherical particles, to detect anisotropic aggregation and to observe the temporal variation of the orientation of an anisotropic object.

## Acknowledgments

The authors acknowledge the financial support of the Canada Foundation for Innovation (CFI), the Natural Sciences and Engineering Research Council of Canada (NSERC), and CREATE. T.G. thanks Canada Research Chair in Liquid Crystals and Behavioral Biophotonics and Manning Innovation prize for financial support. We are grateful to G. Paradis, K. Allahverdyan and Dr. A. Tork (from LensVector and TLCL Optical Research Inc.) for their help during our experiments, to the group of H.C. Berg for bacterial strains, and to Remy Colin for sharing with us his tracking algorithm.

## References

- [1] Viney, C., Huber, A. E., & Verdugo, P. (1993). *Macromolecules*, 26, 852.
- [2] Kupchinov, B. I. et al. (1993). *Smart Mater. Struct.*, 2, 7.
- [3] Stojković, B., Sretenovic, S., Dogsa, I., Poberaj, I., & Stopar, D. (2015). *Biophys. J.*, 108, 758.
- [4] Rey, A. D., Herrera-Valencia, E. E., & Murugesan, Y. K. (2014). *Liq. Cryst.*, 41, 430.
- [5] Giraud-Guille, M.-M. (1998). *Curr. Opin. Solid State Mater. Sci.*, 3, 221.
- [6] Wilding, P. et al. (1994). *Clin. Chem.*, 40, 43.
- [7] Kumar, A., Galstian, T., Pattanayek, S. K., & Rainville, S. (2013). *Mol. Cryst. Liq. Cryst.*, 574, 33.
- [8] Zhou, S., Sokolov, A., Lavrentovich, O. D., & Aranson, I. S. (2014). *Proc. Natl. Acad. Sci.*, 111, 1265.
- [9] Mushenheim, P. C. et al. (2014). *Soft Matter*, 10, 88.
- [10] Mushenheim, P. C., Trivedi, R. R., Weibel, D. B., & Abbott, N. L. (2014). *Biophys. J.*, 107, 255.
- [11] Duchesne, I., Rainville, S., & Galstian, T. (2015). *Biophys. J.*, 109, 2137.
- [12] Duchesne, I., Galstian, T., & Rainville, S. (2014). *SPIE Proceeding*, 9182, 91820M.
- [13] Berg, H. C. & Turner, L. (1979). *Nature*, 278, 349.
- [14] Senyuk, B., Glugla, D., & Smalyukh, I. I. (2013). *Phys. Rev. E*, 88, 062507.
- [15] Ivlev, A. V. et al. (2007). *Phys. Rev. Lett.*, 98, 145003.
- [16] Wolfe, A. J. & Berg, H. C. (1989). *Proc. Natl. Acad. Sci. U. S. A.*, 86, 6973.
- [17] Prasad, S. K., Nair, G. G., Hegde, G., & Jayalakshmi, V. (2007). *J. Phys. Chem. B*, 111, 9741.
- [18] Stark, H. & Ventzki, D. (2001). *Phys. Rev. E*, 64, 031711.
- [19] Loudet, J. C., Hanusse, P., & Poulin, P. (2004). *Science*, 306, 1525.
- [20] Mondiot, F., Chandran, S. P., Mondain-Monval, O., & Loudet, J.-C. (2009). *Phys. Rev. Lett.*, 103, 238303.
- [21] Turiv, T. et al. (2013). *Science*, 342, 1351.
- [22] Saveyn, H. et al. (2010). *J. Colloid Interface Sci.*, 352, 593.
- [23] Seo, D. S., Matsuda, H., Oh-ide, T., & Kobayashi, S. (1993). *Mol. Cryst. Liq. Cryst. Sci. Technol. Sect. Mol. Cryst. Liq. Cryst.*, 224, 13.
- [24] Smalyukh, I. I., Lavrentovich, O. D., Kuzmin, A. N., Kachynski, A. V., & Prasad, P. N. (2005). *Phys. Rev. Lett.*, 95, 157801.
- [25] Zhou, S. et al. (2014). *Soft Matter*, 10, 6571.
- [26] M. Blinov, L. (2011). *Structure and Properties of Liquid Crystals*, Springer: New York, NY.
- [27] Berezhkovskii, A. M., Dagdug, L., & Bezrukov, S. M. (2014). *Biophys. J.*, 106, L09.
- [28] Lundblad, R. L. & Macdonald, F. M. (2010). *Handbook of Biochemistry and Molecular Biology*, 4th ed. CRC Press: Boca Raton, FL.
- [29] Kostko, A. F. et al. (2005). *J. Phys. Chem. B*, 109, 19126.
- [30] Lydon, J. (2011). *Liq. Cryst.*, 38, 1663.